Available online at www.sciencedirect.com
SCIENCE DIRECT
Physics Letters A 349 (2006) 388–392
PHYSICS LETTERS A
www.elsevier.com/locate/pla

Destabilization of the cooperative Jahn–Teller effect in $Sr_{0.9}Ce_{0.1}MnO_3$ by Cr-doping

W.J. Lu *, Y.P. Sun, X.B. Zhu, W.H. Song, J.J. Du

Key Laboratory of Materials Physics, Institute of Solid State Physics, Chinese Academy of Sciences, Hefei 230031, PR China

Received 11 September 2005; accepted 14 September 2005

Available online 21 September 2005

Communicated by V.M. Agranovich

Abstract

The structural study of $Sr_{0.9}Ce_{0.1}Mn_{1-y}Cr_yO_3$ ($y = 0$, 0.05, and 0.10) has been carried out by X-ray diffraction. For undoped sample $Sr_{0.9}Ce_{0.1}MnO_3$, it undergoes a first-order structural transition accompanied by Jahn–Teller (JT) transition at $T_{JT} = 320$ K. The JT transition temperature is reduced in Cr-doped samples, becoming $T_{JT} = 260$ K for $y = 0.10$. The tetragonal $I4/mcm$ structure is characterized by the JT distortion in MnO_6 octahedra with the distortion mode Q_3. With increasing Cr doping content, the deformation of MnO_6 octahedra is weakened, showing that Cr doping destabilizes the JT effect. In addition, elastic properties measurement indicates that a large softening of Young's modulus occurs in the vicinity of T_{JT}, which has been interpreted in terms of the strong electron–phonon coupling originating from the JT effect.

PACS: 75.47.Lx; 71.70.Ej; 63.20.Kr

Keywords: Manganites; Jahn–Teller effect; Electron–phonon interaction

1. Introduction

Colossal magnetoresistance (CMR) in the manganites $R_{1-x}A_xMnO_3$ (R = rare-earth ions; A = divalent ions) with mixed Mn^{3+}/Mn^{4+} valence has become a focus of recent studies in view of their special electronic and magnetic properties as well as the potential applications. The feature of the CMR manganites is the strong interaction between charge carriers in the e_g band, localized spins of t_{2g} electrons, and the crystal lattice. Initially, the double exchange (DE) interaction between Mn^{3+} and Mn^{4+} introduced by Zener [1] can explain the electrical and magnetic properties qualitatively. However, a recent calculation by Millis et al. [2,3] indicated that the DE model alone could not explain resistivity and CMR effects quantitatively. In addition to DE model, a lattice polaron due to a strong electron–phonon interaction plays an important role. Especially, they claimed that the lattice distortion due to the Jahn–Teller (JT) splitting of e_g electrons is important. There have been lots of experimental works [4,5], which suggest importance of the electron–phonon coupling in the manganites.

The clearest evidence of the JT effect in the perovskites happens in the parent compound, $LaMnO_3$. At room temperature, this compound is an A-type antiferromagnetic (AFM) insulator in which a cooperative JT effect in the MnO_6 octahedra induces an orbital ordering. Above $T_{JT} \approx 750$ K [6,7] the structure of $LaMnO_3$ becomes quasi-cubic, in which the MnO_6 octahedra are quasi-regular. Chatterji et al. [8] have systematically investigated the doping dependence of the JT transition in $La_{1-x}Sr_xMnO_3$ ($0 < x \leqslant 0.1$). They found that the JT transition temperature is drastically reduced on doping with Sr. Over the past decade the structural, electrical, and magnetic properties of the hole-doped manganites have been studied in the greatest detail. In contrast to the hole-doped manganites, the electron-doped manganites (such as Ce doped $CaMnO_3$ or $SrMnO_3$) have been an interesting system [9–12]. It is a very important field for structural investigations in order to understand the role of JT effect on the magnetic and transport properties of these oxides.

* Corresponding author.
E-mail addresses: wjlu@issp.ac.cn (W.J. Lu), ypsun@issp.ac.cn (Y.P. Sun).

0375-9601/$ – see front matter
doi:10.1016/j.physleta.2005.09.037

A recent study of the Mn sites doping in $R_{1-x}A_xMnO_3$ has revealed that Cr has a spectacular effect in the magnetic and transport properties. For instance, the Cr doping in the charge ordered (CO) insulator $Pr_{0.5}Ca_{0.5}MnO_3$ can destroy the CO AFM state and induce a metal–insulator (M–I) transition [13,14]. The Cr substitution in electron-doped $Ca_{0.9}Ce_{0.1}MnO_3$ leads to the coexistence of ferromagnetic (FM) and AFM phases and the observations of cluster glass behavior [15]. Very recently, we synthesized the Cr doped $Sr_{0.9}Ce_{0.1}MnO_3$ samples and studied the electrical and magnetic properties associated with JT transition [16]. The change of electrical and magnetic properties due to Cr doping has been attributed to the weakening of JT distortion. In order to check whether the JT distortion is weakened by Cr doping, structural investigations as a function of temperature are required. In present Letter, we give a direct evidence of JT distortion of the MnO_6 octahedra by X-ray diffraction in large temperature range. The results indicate that Cr doping destabilizes the JT effect. The anomalous Young's modulus properties imply the electron–phonon coupling due to the JT effect may play an important role in the system.

2. Experimental

Polycrystalline $Sr_{0.9}Ce_{0.1}Mn_{1-y}Cr_yO_3$ ($y = 0$, 0.05, and 0.10) samples were synthesized by the standard solid-state reaction. Stoichiometric precursor powders $SrCO_3$, CeO_2, MnO_2 and Cr_2O_3 were mixed and ground, then fired for 24 h at 1050 °C. The resultant powder was then pressed into small pellets and sintered at 1200 °C for 24 h and then at 1350 °C for another 24 h. After the final grinding, the powder was pressed into bars with the dimension of $65.0 \times 4.5 \times 1.0$ mm^3 (for Young's modulus measurements), sintered at 1400 °C for 24 h and slow-cooled to room temperature.

X-ray diffraction (XRD) measurement was taken by Philips X'pert PRO X-ray diffractometer with Cu K_α radiation. The structural parameters were obtained by fitting the experimental data of XRD using the standard Rietveld technique. Young's modulus $E(T)$ were measured by the electrostatic drive and capacitor microphone detection technique [17], which makes it possible to obtain the resonant frequency. The Young's modulus E is given by

$$E = \frac{4\pi^2 s d l^4}{m^4 I} f^2, \tag{1}$$

where f is the resonant frequency, s the cross-sectional area, d the density, l the length, I the moment of inertia of the sample. In addition, m is 4.730 for the vibrating mode in the fundamental mode. The measurement was made in acoustic frequency range with magnitude of kHz using warming mode in a vacuum environment at the rate of 1 K/min.

3. Results and discussion

The analysis of XRD patterns indicates that a structural phase transition from cubic to tetragonal due to JT ordering occurs at T_{JT} for all samples. The JT transition temperature T_{JT} are 320, 290, and 260 K for $y = 0$, 0.05, and 0.10, respectively.

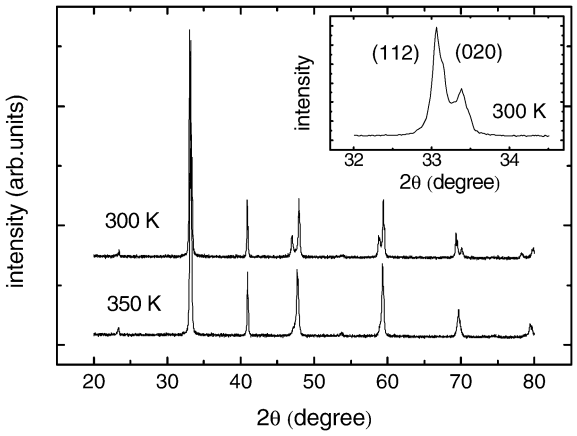

Fig. 1. X-ray diffraction patterns of $Sr_{0.9}Ce_{0.1}MnO_3$ at 300 and 350 K. The inset shows (112) and (020) reflections of the tetragonal phase at 300 K.

Above T_{JT} the unit cell is cubic $Pm3m$ lattice and below T_{JT} the reflections can be indexed by tetragonal $I4/mcm$ lattice. The volume of the tetragonal unit cell is four ($\sqrt{2} \times \sqrt{2} \times 2$) times that of the cubic unit cell. As an example, Fig. 1 shows the XRD patterns at two selected temperatures (300 and 350 K) for undoped $Sr_{0.9}Ce_{0.1}MnO_3$. At 350 K, the structure of this sample is cubic, where no lattice distortion exists. Upon cooling, the structure changes to tetragonal lattice with static JT distortion at 300 K. The (112) and (020) reflections of the low-temperature tetragonal phase can be clearly seen at 300 K in the inset of Fig. 1. For all samples, the electrical and magnetic properties associated with JT transition have been studied in our previous work [16]. Above T_{JT}, the resistivity is low and is independent of temperature down to 320 K. This is in agreement with the fact that the high-temperature structure is cubic where the doped electrons occupy the degenerate e_g band and is responsible for metallic conductivity. Below T_{JT}, the resistivity increases logarithmically with decreasing temperatures. The insulating behavior in the tetragonal phase is consistent with the localization of doping electrons due to the strong JT distortion.

The refined lattice parameters as a function of temperature are shown in Fig. 2. For all samples, in tetragonal phase a decreases and c increases with decreasing temperatures. The mismatch between a and c is enhanced by decreasing temperatures. In other words, the lattice distortion increases at lower temperatures. On the other hand, Cr doping weakens the mismatch between a and c. For instance, at 200 K the values of mismatch are 2.4194, 2.3307, and 2.2923 Å for $y = 0$, 0.05, and 0.10, respectively. The mismatch disappears abruptly as the cell structure changes to cubic upon heating. The drastic change of the structure implies the first-order transition in the samples.

Concentrating first on the low-temperature phase, we observe a permanent or static distortion below T_{JT} that results in MnO_6 octahedra with two different Mn–O lengths. In Table 1 we have summarized the geometrical parameters of undoped $Sr_{0.9}Ce_{0.1}MnO_3$ that are directly related to JT effect. There are two different bond lengths and angles. At 300 K, the two longer Mn–O1 bond length is 1.935(2) Å, and the four shorter Mn–O2 bond length is 1.913(1) Å. The difference between them is $\Delta d = 0.022$ Å, which is regarded as the distortion

parameter of JT distortion in MnO_6 octahedra. This value of distortion parameters Δd increases with decreasing temperatures. At 100 K Δd gets to 0.071 Å, which indicates that there is a strong JT distortion in MnO_6 octahedra and the doping electrons occupy the $d_{3z^2-r^2}$ orbital of JT split state (elongated octahedra). Below T_{JT}, the orbital ordering is established due to the cooperative JT effect breaking the degeneracy of the electronic configuration of Mn^{3+}. This particular orbital ordering is responsible for C-type magnetic structure described in the experimental work by Sundaresan et al. [11]. On the other hand, the Mn–O1–Mn bond angle remains 180 degrees and the Mn–O2–Mn angle is smaller than 180 degrees. This is in agreement with the rotation of the octahedron along the c-axis in opposite direction in the successive planes for $I4/mcm$ space group. In Table 1, we can clearly see that the Mn–O2–Mn bond angle deviates from 180 degrees and decreases with decreasing temperatures. Accordingly, the bending angle of Mn–O2–Mn increases from $\Delta\theta = 2.52°$ at 300 K to $\Delta\theta = 7.55°$ at 100 K. The bending of Mn–O–Mn bond angle modifies the strength of the hopping integral between e_g(Mn)–$2p_\sigma$(O)–e_g(Mn) orbitals and, therefore, the electronic bandwidth [18,19]. Therefore, the bending of Mn–O–Mn bond angle is responsible for the insulator state of $Sr_{0.9}Ce_{0.1}MnO_3$ in low-temperature tetragonal phase [16].

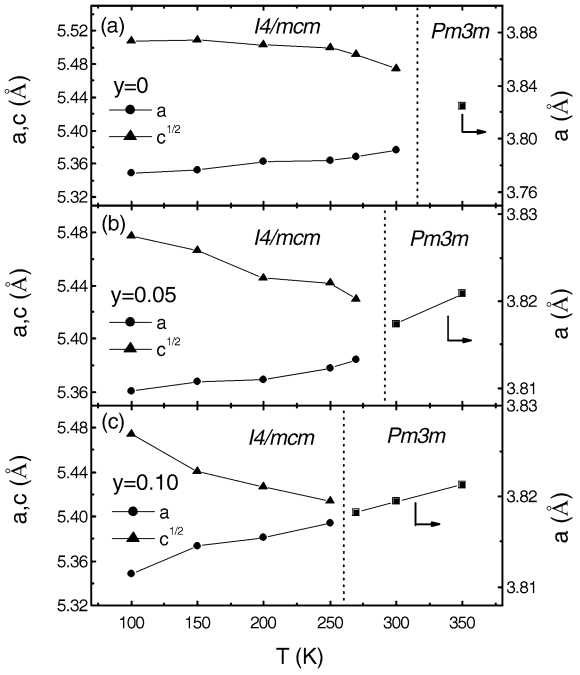

Fig. 2. Temperature dependence of the lattice parameters of $Sr_{0.9}Ce_{0.1}Mn_{1-y}Cr_yO_3$ for (a) $y = 0$, (b) 0.05, and (c) 0.10. The structural transition due to Jahn–Teller ordering is marked with the dotted lines.

Above T_{JT}, the MnO_6 octahedra become nearly regular in the high-temperature cubic phase. At 350 K, the Mn–O bond lengths are 1.9123(3), 1.9115(3), and 1.9107(2) Å for $y = 0$, 0.05, and 0.10, respectively. For the samples with different Cr doping content, the Mn–O bond lengths of the regular MnO_6 octahedra are very close from each other, which is due to the small difference in ionic size between Mn^{3+} (0.645 Å) and Cr^{3+} (0.615 Å) ions and only small values of the level of substitutions (up to 10%). Although no static JT distortion in MnO_6 octahedra has been observed, the existence of a dynamic JT distortion cannot be ruled out. For $LaMnO_3$ [20], at $T > 750$ K the MnO_6 octahedra keep their local distortion and the JT transition would only indicate a change from a static and cooperative distortion to dynamic and local distorted octahedra. The observed average cubic lattice in $Sr_{0.9}Ce_{0.1}Mn_{1-y}Cr_yO_3$ is probably the result of dynamic spatial fluctuations of the underlying tetragonal distortion. It needs further experimental results to support the hypothesis that JT transition would correspond to change from a static distortion to a dynamic one, without removing of the local distortions present in the MnO_6 octahedra.

Fig. 3 shows the distortion parameters Δd and $\Delta\theta$ at several selected temperatures in the tetragonal phase for all samples. As discussed above, the JT distortion of MnO_6 octahedra increases with decreasing temperatures, considering the continuous increase of Δd and $\Delta\theta$. The distortion of MnO_6 octahedra at a

Table 1
Refined structural parameters of $Sr_{0.9}Ce_{0.1}MnO_3$ at several selected temperatures. Space group $I4/mcm$, Sr and Ce in $4b(0, 1/2, 1/4)$, Mn in $4c(0, 0, 0)$, O1 in $4a(0, 0, 1/4)$, O2 in $8h(x, y, 0)$. ⟨Mn–O⟩ is the average Mn–O bond length. ⟨Mn–O–Mn⟩ is the average Mn–O–Mn bond angle. The distortion parameter $\Delta d = d_1 - d_2$ (d_1 = Mn–O1, d_2 = Mn–O2). The distortion parameter $\Delta\theta = \theta_1 - \theta_2$ (θ_1 = Mn–O1–Mn, θ_2 = Mn–O2–Mn)

	300 K	250 K	200 K	150 K	100 K
a, b (Å)	5.3770(3)	5.3636(4)	5.3615(2)	5.3529(2)	5.3492(4)
c (Å)	7.7407(5)	7.7761(6)	7.7809(5)	7.7899(4)	7.7877(8)
V (Å^3)	223.800(4)	223.704(3)	223.667(2)	223.208(2)	222.837(3)
x (O2)	0.243(2)	0.239(2)	0.238(1)	0.241(3)	0.236(1)
y (O2)	0.746(3)	0.741(4)	0.739(2)	0.735(4)	0.731(4)
Mn–O1 × 2 (Å)	1.935(2)	1.944(2)	1.945(2)	1.947(3)	1.947(4)
Mn–O2 × 4 (Å)	1.913(1)	1.905(2)	1.898(1)	1.879(1)	1.876(2)
⟨Mn–O⟩ (Å)	1.924	1.925	1.922	1.913	1.912
Δd (Å)	0.022	0.039	0.047	0.068	0.071
Mn–O1–Mn (°)	180.00(1)	180.00(2)	180.00(5)	180.00(4)	180.00(5)
Mn–O2–Mn (°)	177.48(7)	175.42(8)	174.96(6)	174.50(6)	172.45(10)
⟨Mn–O–Mn⟩ (°)	178.74	177.71	177.48	177.25	176.23
$\Delta\theta$ (°)	2.52	4.58	5.04	5.50	7.55
R_P (%)	5.95	4.62	4.52	4.87	4.97
R_{exp} (%)	4.11	3.32	3.03	4.02	3.30

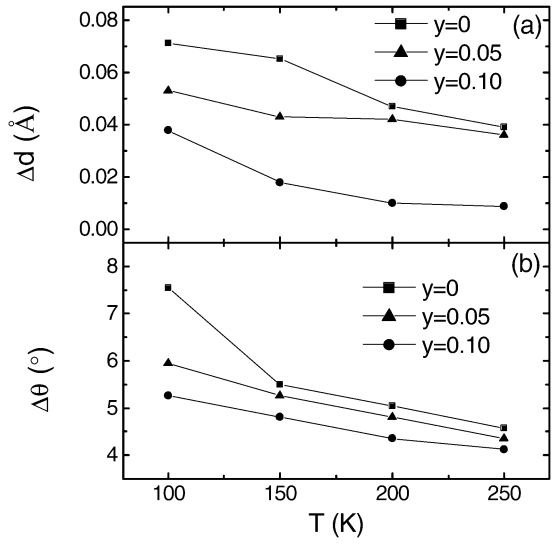

Fig. 3. Temperature dependence of distortion parameters (a) $\Delta d = d_1 - d_2$ and (b) $\Delta\theta = \theta_1 - \theta_2$ in low-temperature tetragonal phase.

particular temperature is reduced with increasing doping content y. In other words, JT distortion is weakened by Cr doping. In order to study the Cr doping effect on JT distortion further, we study the elastic properties by Young's modulus measurement for all samples. Young's modulus microscopically reflects the strain among the atoms. For isotropic materials such as polycrystalline samples, Young's modulus E is given by:

$$E = \frac{C_{44}(C_{11} + 2C_{12})}{C_{12} + C_{44}} = \frac{\mu(3\lambda + 2\mu)}{\lambda + \mu}, \tag{2}$$

$$\lambda + 2\mu = C_{11}, \qquad \lambda = C_{12}, \qquad \mu = C_{44}, \tag{3}$$

where λ and μ are Lamé's constants and C_{ij} the tensor component of the elastic stiffness constant. Elastic constants are very sensitive to structural phase transition, the elastic constant softening is the soft mode associated with the transition and reflects the instability of the lattice to a strain of a given symmetry [21,22]. The experimental results of the relative Young's modulus ΔE ($\Delta E = E(T)/E_{\min}$) are shown in Fig. 4. For all samples, ΔE comes into being a valley and reaches a minimum value at T_P. The values of T_P are very close to the JT transition temperatures T_{JT}. Undoubtedly, the softening of Young's modulus in the vicinity of T_{JT} should be due to the JT transition accompanied by an orbital order–disorder transition. The $3d$ electron state of transition-metal ions has an electric quadrupole moment due to the orbital state as well as a magnetic dipole moment. The softening of Young's modulus should originate from the coupling of the orbital (quadrupolar) moment of the e_g orbital, $d_{3z^2-r^2}$ and $d_{x^2-y^2}$, of Mn^{3+} ion to the elastic strain [23]. Therefore, this simultaneous occurrence of electron ordering and lattice softening implies that extremely strong electron–phonon coupling due to the JT effect may play an important role in the samples. On the other hand, the degree of softening of E is reduced due to Cr doping. As an example, in Table 2 we compare the relative modulus ΔE with the JT distortion parameters Δd and $\Delta\theta$ at 200 K for all samples. At 200 K the values of ΔE are 2.42, 1.73, and 1.25 for $y = 0$, 0.05, and 0.10, respectively. The continuous decrease of ΔE is consistent with

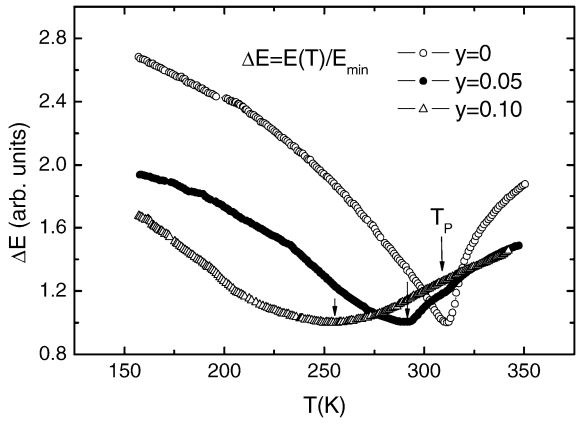

Fig. 4. Temperature dependence of relative Young's modulus ΔE ($= E(T)/E_{\min}$) for $Sr_{0.9}Ce_{0.1}Mn_{1-y}Cr_yO_3$ ($y = 0$, 0.05, and 0.10). T_P is defined as the temperature at which ΔE reaches a minimum.

Table 2
Structural parameters obtained by Rietveld refinements of X-ray diffraction data of $Sr_{0.9}Ce_{0.1}Mn_{1-y}Cr_yO_3$ ($y = 0$, 0.05, and 0.10) at selected temperature 200 K. The relative Young's modulus ΔE is defined as $\Delta E = E(T)/E_{\min}$. The values of ΔE are obtained from Fig. 4

	$y = 0$	$y = 0.05$	$y = 0.10$
a (Å)	5.3615(2)	5.3692(4)	5.3813(3)
c (Å)	7.7809(5)	7.6999(4)	7.6736(4)
V (Å^3)	223.667(2)	221.975(3)	222.215(3)
⟨Mn–O⟩ (Å)	1.922	1.903	1.913
⟨Mn–O–Mn⟩ (°)	177.48	177.60	177.83
Δd (Å)	0.047	0.044	0.01
$\Delta\theta$ (°)	5.04	4.81	4.35
ΔE	2.42	1.73	1.25

the decrease of distortion parameters, indicating that the magnitude of ΔE is proportional to the fraction of the Q_3-type JT distortion [24]. Therefore, the decrease of ΔE with increasing Cr doping content shows that Cr doping weakens the JT distortion of MnO_6 octahedra. That is to say, the cooperative JT effect is destabilized by Cr doping.

4. Conclusion

In summary, a JT transition associated with orbital order–disorder transition has been observed in $Sr_{0.9}Ce_{0.1}Mn_{1-y}Cr_yO_3$ ($y = 0$, 0.05, and 0.10). Due to Cr doping, the JT transition temperature T_{JT} decreases from 320 K for undoped sample to 260 K for doped sample with $y = 0.10$. The JT distortion of MnO_6 octahedra is weakened by Cr doping. A large softening of Young's modulus in the vicinity of T_{JT} indicates that the strong electron–phonon interaction originating from the JT effect may play an important role in the samples.

Acknowledgements

This work was supported by the National Key Research under Contract No. 001CB610604, and the National Nature Science Foundation of China under Contract Nos. 10374033 and

10474100, and the Fundamental Bureau, Chinese Academy of Sciences.

References

[1] C. Zener, Phys. Rev. 82 (1951) 403.
[2] A.J. Millis, P.B. Littlewood, B.I. Shraiman, Phys. Rev. Lett. 74 (1995) 5144.
[3] A.J. Millis, B.I. Shraiman, R. Mueller, Phys. Rev. Lett. 77 (1996) 175.
[4] P. Dai, J. Zhang, H.A. Mook, S.J. Liou, P.A. Dowben, E.W. Plummer, Phys. Rev. B 54 (1996) 3694.
[5] G. Zhao, K. Conder, H. Keller, K.A. Muller, Nature 381 (1996) 676.
[6] J.-S. Zhou, J.B. Goodenough, Phys. Rev. B 60 (1999) R15002.
[7] J. Rodríguez-Carvajal, M. Hennion, F. Moussa, A.H. Moudden, L. Pinsard, A. Revcolevschi, Phys. Rev. B 57 (1998) R3189.
[8] T. Chatterji, B. Ouladdiaf, P. Mandal, B. Bandyopadhyay, B. Ghosh, Phys. Rev. B 66 (2002) 054403.
[9] Z. Zeng, M. Greenblatt, M. Croft, Phys. Rev. B 63 (2001) 224410.
[10] P. Mandal, A. Hassen, A. Loidl, Phys. Rev. B 69 (2004) 224418.
[11] A. Sundaresan, J.L. Tholence, A. Maignan, C. Martin, M. Hervieu, B. Raveau, E. Suard, Eur. Phys. J. B 14 (2000) 431.
[12] J.W. Lynn, R.W. Erwin, J.A. Borchers, Q. Huang, A. Santoro, J.-L. Peng, Z.Y. Li, Phys. Rev. Lett. 76 (1996) 4046.
[13] F. Damay, C. Martin, A. Maignan, M. Hervieu, B. Raveau, F. Bourée, G. André, Appl. Phys. Lett. 73 (1998) 3772.
[14] R. Mahendiran, B. Raveau, M. Hervieu, C. Michel, A. Maignan, Phys. Rev. B 64 (2001) 064424.
[15] R. Ganguly, M. Hervieu, A. Maignan, C. Martin, B. Raveau, J. Phys.: Condens. Matter 14 (2002) 9039.
[16] W.J. Lu, B.C. Zhao, R. Ang, W.H. Song, J.J. Du, Y.P. Sun, Solid State Commun., in press.
[17] F.Y.X. Chen, P. Bao, Y. Wang, J. Liu, J. Appl. Phys. 87 (2000) 1453.
[18] J. Fontcuberta, B. Martínez, A. Seffar, S. Piñol, J.L. García-Muñoz, X. Obradors, Phys. Rev. Lett. 76 (1996) 1122.
[19] H.Y. Hwang, S.-W. Cheong, P.G. Radaelli, M. Marezio, B. Batlogg, Phys. Rev. Lett. 75 (1995) 914.
[20] E. Araya-Rodriguez, A.Y. Ramos, H.C.N. Tolentino, E. Granado, S.B. Oseroff, J. Magn. Magn. Mater. 233 (2001) 88.
[21] M. Kataoka, J. Phys. Soc. Jpn. 70 (2001) 2353.
[22] M. Saint-Paul, P. Lejay, Physica B 352 (2004) 353.
[23] Y.Q. Ma, W.H. Song, R.L. Zhang, J.M. Dai, J. Yang, J.J. Du, Y.P. Sun, C.Z. Bi, Y.J. Ge, X.G. Qiu, Phys. Rev. B 69 (2004) 134404.
[24] R.K. Zheng, G. Li, A.N. Tang, Y. Yang, W. Wang, X.G. Li, Z.D. Wang, H.C. Ku, Appl. Phys. Lett. 83 (2003) 5250.